

# Non Fermi liquid signatures across strain engineered metal-insulator transition in line-graph lattices

Shashikant Singh Kunwar<sup>1</sup> and Madhuparna Karmakar<sup>2,\*</sup>

<sup>1</sup>*Department of Physics and Astronomy, University of Iowa,  
Iowa City, Iowa 52242, United States of America*

<sup>2</sup>*Department of Physics and Nanotechnology, SRM Institute of Science and Technology,  
Kattankulathur, Chennai 603203, India*

(Dated: February 24, 2026)

Controlling the properties and thus the functionalities of correlated electron systems via externally tunable perturbations has always remained a cherished goal in quantum condensed matter physics. Recently, straintronics has proved to be one such external control which can dictate the quantum phases and transitions in materials via the reconstruction of their electronic band structure. A particularly intriguing scenario arises in the context of flat band line-graph lattices wherein straintronics is found to bring forth non trivial phase transitions. This paper reports the phase transitions and thermal scales across the Lieb/Kagome interconversion in the electronic interaction-strain-temperature space. Based on the thermodynamic, spectroscopic and transport signatures across the strain tuned interconversion of these line-graph lattices we have mapped out the low temperature phases and thermal transition scales, numerically determined using non perturbative calculations. While at the low temperatures, interaction-strain plane is spanned by magnetically correlated insulators, flat band induced weak transiently localized insulators and non Fermi liquid metallic phases, thermal fluctuations aid in to stabilize coexistent magnetic correlations. Apart from quantifying the magnetic transition scales in this system our results on the spectroscopic and transport signatures distill the strain tuned metal-insulator transition and crossover scales which exhibit variable transport scaling exponents.

## I. INTRODUCTION

Quantum materials are inherently sensitive to the external perturbations bringing forth via band structure reconstruction; exotic phases, their competition and the scales associated therein. A particularly intriguing scenario arises in geometrically frustrated materials with multiple electronic bands and flat bands. An example being the Kagome metal, currently in vogue owing to its recent material realization and prospective artificial engineering<sup>1-31</sup>. Interestingly, the Kagome lattice shares many of its characteristics with another line-graph lattice viz. the Lieb lattice<sup>32-37</sup>.

Naturally, there has been a flurry of research to look for a potential tuning parameter or perturbation which not just aids in to smoothly traverse from one lattice to the other but is experimentally accessible. In this quest the perturbation which has repeatedly made its appearance in the literature is the applied strain, experimentally accessible and a clean substitute of chemical doping or disorder. Based on the non interacting model Hamiltonian it was shown that straintronics across the Lieb/Kagome interconversion leads to emergent Dirac cones via the deconstruction and the eventual reconstruction of the electronic band structure. The system undergoes topological phase transition across this interconversion which are quantified in terms of Chern number<sup>32-37</sup>. These noninteracting toy models are however, far removed from the practical Lieb or Kagome materials where electronic correlations dominate the physics and geometric frustration allows for novel quantum phases and phase competitions, as have been observed in the recently discovered Kagome materials such as,  $\text{Mn}_3\text{Sn}$ <sup>1-6</sup>,  $\text{Fe}_3\text{Sn}_2$ <sup>7-14</sup>,  $\text{Co}_3\text{Sn}_2\text{S}_2$ <sup>15-21</sup>,  $\text{Gd}_3\text{Ru}_4\text{Al}_{12}$ <sup>22,23</sup>,  $\text{FeSn}$ <sup>24-27</sup> and the  $\text{AV}_3\text{Sb}_5$  series ( $A = \text{K, Rb, Cs}$ )<sup>28,29</sup>.

A possible engineered set up to realize this lattice interconversion is the metal organic framework (MOF)

which is a promising avenue owing to its broad tunability in terms of material composition, topology and choice of substrates, all of which contribute to their advance functionalities<sup>30,31</sup>. The Lieb and Kagome band structures serve as the fundamental structural motifs of two-dimensional (2D) MOF. They have been experimentally realized in compounds such as, 9,10-dicyanoanthracene-copper (DCA-Cu)<sup>31,38,39</sup>,  $\text{MCl}_2(\text{pyrazine})_2$ <sup>40</sup>, and 1,2,4,5-tetracyanobenzene (TCNB)<sup>41</sup>.

Numerical investigation of the quantum phases in presence of strong electronic correlations across this interconversion is a formidable task. This is particularly true in the Kagome limit where strong geometric frustration along with the multiple electronic bands in these materials render the existing non perturbative numerical approaches redundant, owing to severe fermionic sign problem and system size restrictions<sup>42-53</sup>. Recently we have demonstrated that such numerical constrains can be eased out to an extent based on the static path approximated (SPA) Monte Carlo technique which allows one to access the low temperature physics of these systems for a reasonably large system size<sup>54,55</sup>. Based on the half filled Kagome Hubbard model (KHM) with the anisotropic nearest neighbor hopping amplitudes mimicking the applied strain, it was shown that in the weak coupling regime continuous tuning of the applied strain leads to a re-entrant metal-insulator transition and crossover. The intermediate strain regime hosts a non Fermi liquid (NFL) metal cradled between a gapped and a gapless insulating phases<sup>55</sup>.

In this paper we take a step further in this direction and investigate the comprehensive three-dimensional interaction-strain-temperature ( $U - \eta - T$ ) parameter space across the Lieb/Kagome interconversion. The system is modeled using the half filled KHM with anisotropic hopping, which we analyze in terms of our extensive results on the thermodynamic,

spectroscopic and transport signatures of this system. Our primary inferences based on this work include: (i) applied strain in the interaction plane brings forth magnetically correlated insulators, NFL metal and flat band induced weakly localized insulating phases, (ii) the metal-insulator transition and crossover in this system are controlled by the applied strain with the variable scaling exponents of the electronic transport signatures attesting to the deviation from the Fermi liquid description, (iii) thermal fluctuations promote thermodynamic phases with competing and coexisting magnetic order via stabilizing short range sub-dominant magnetic correlations.

The remaining of this paper is structured as follows: in Section 2 we discuss the model Hamiltonian and the numerical approach used to understand the transitions in the  $U - \eta - T$  space, along with the relevant indicators to characterize the thermodynamic phases and phase transitions. Section 3 contain the results of this work presented in terms of the low temperature signatures while Section 4 discusses the finite temperature phases and the thermal scales. We conclude in Section 5 following a discussion of our observations and their potential applications.

## II. MODEL AND METHOD

We model this multiband system using the 2D Hubbard Hamiltonian defined on the strain tuned Lieb/Kagome lattice<sup>47,48,54</sup>,

$$\hat{H} = - \sum_{\langle ij \rangle, \sigma} t_{ij} (\hat{c}_{i,\sigma}^\dagger \hat{c}_{j,\sigma} + h.c.) - \eta \sum_{\langle ij \rangle, \sigma} (\hat{c}_{i,\sigma}^\dagger \hat{c}_{j,\sigma} + h.c.) - \mu \sum_{i,\sigma} \hat{n}_{i\sigma} + U \sum_i \hat{n}_{i\uparrow} \hat{n}_{i\downarrow} \quad (1)$$

Here,  $t_{ij} = t = 1$  represents the hopping amplitude between nearest-neighbors and sets the reference energy scale for the system. The parameter  $\eta$  characterizes the applied shear strain, allowing interpolation between the Lieb ( $\eta = 0$ ) and the Kagome ( $\eta = 1$ ) limits. The on-site Hubbard interaction is given by  $U > 0$ , and the chemical potential  $\mu$  is tuned to ensure a half-filled lattice. To render the model computationally tractable, the interaction term is decoupled using the Hubbard-Stratonovich (HS) transformation<sup>56,57</sup>, which introduces auxiliary bosonic fields: a vector field  $\mathbf{m}_i(\tau)$  that couples to the spin and a scalar field  $\phi_i(\tau)$  that couples to the charge<sup>54</sup>. SPA is based on the adiabatic (slow boson) approximation wherein the bosonic fields are treated as classical, serving as a static, randomly fluctuating disordered background to the fast moving fermions<sup>58-60</sup>. The adiabatic approximation allows us to access the real frequency dependent quantities without requiring an analytic continuation. This is particularly useful in accessing the low temperature physics of geometrically frustrated systems such as, Kagome materials. The adiabatic approximation is valid for  $T > T_{FL}$  where,  $T_{FL}$  corresponds to the Fermi liquid coherence temperature<sup>54,58-60</sup>.

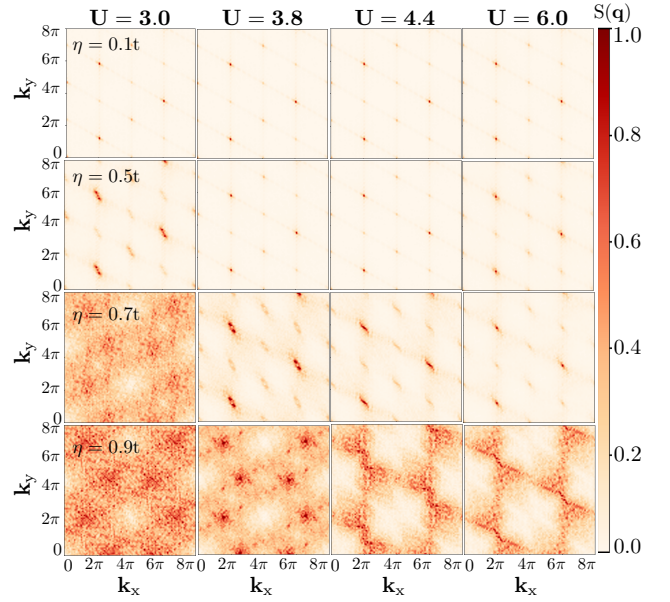


FIG. 1. Static magnetic structure factor ( $S(\mathbf{q})$ ) at  $T = 0.01t$  for selected  $U - \eta$  cross sections. At large strain, magnetic correlations set in for  $U > 3t$ , the intermediate interaction  $U = 3.8t$  hosts a precursor Coulomb phase while the strong coupling regime ( $U = 4.4t$  and  $U = 6.0t$ ) is characterized by a Coulomb phase.

Within the framework of SPA, the  $\phi_i$  field is treated at the saddle point level such that,  $\phi_i \rightarrow \langle \phi_i \rangle = \langle n_i \rangle U/2$  (where  $\langle n_i \rangle$  is the number density of the fermions), while the complete spatial fluctuations of the  $\mathbf{m}_i$  field are retained. The resulting effective Hamiltonian reads as<sup>54,55</sup>,

$$\hat{H}_{eff} = -t \sum_{\langle ij \rangle, \sigma} (\hat{c}_{i\sigma}^\dagger \hat{c}_{j\sigma} + h.c.) - \eta \sum_{\langle ij \rangle, \sigma} (\hat{c}_{i\sigma}^\dagger \hat{c}_{j\sigma} + h.c.) - \tilde{\mu} \sum_{i\sigma} \hat{n}_{i\sigma} - \frac{U}{2} \sum_i \mathbf{m}_i \cdot \sigma_i + \frac{U}{4} \sum_i m_i^2 \quad (2)$$

where, the final term in  $H_{eff}$  accounts for the stiffness cost of the classical bosonic field  $\mathbf{m}_i$ ;  $\sigma_i = \sum_{a,b} \hat{c}_{ia}^\dagger \sigma_{ab} \hat{c}_{ib} = \mathbf{s}_i$  represents the fermions<sup>54,55</sup>. The various phases are characterized based on the fermionic correlators: (i) static magnetic structure factor,  $S(\mathbf{q}) = \frac{1}{N^2} \sum_{ij} \langle \mathbf{m}_i \cdot \mathbf{m}_j \rangle e^{i\mathbf{q} \cdot (\mathbf{r}_i - \mathbf{r}_j)}$ , where  $\mathbf{q}$  corresponds to the magnetic ordering wave vector and  $N$  is the number of lattice sites. The notation  $\langle \dots \rangle$  denotes the Monte Carlo configurational average. (ii) Single particle density of states (DOS),  $N(\omega) = (1/N) \sum_n \langle \delta(\omega - \epsilon_n) \rangle$  where,  $\epsilon_n$  are the eigenvalues of a single equilibrium configuration. (iii) Optical conductivity,  $\sigma(\omega) = \frac{\sigma_0}{N} \sum_{\alpha,\beta} \frac{f(\epsilon_\alpha) - f(\epsilon_\beta)}{\epsilon_\beta - \epsilon_\alpha} |\langle \alpha | J_x | \beta \rangle|^2 \delta(\omega - (\epsilon_\beta - \epsilon_\alpha))$ , where, the current operator  $J_x$  is defined as,  $J_x = -i \sum_{i,\sigma,\delta} [\delta_{i\sigma}^\dagger c_{\mathbf{r}_i,\sigma} c_{\mathbf{r}_i+\delta,\sigma} - H.c.]$ , with  $f(\epsilon_\alpha)$  being the Fermi function and  $\epsilon_\alpha$  and  $|\alpha\rangle$  are respectively, the single particle eigenvalues and eigenvectors of  $H_{eff}$  in a given background of  $\{\mathbf{m}_i\}$ . (iv) dc conductivity,  $\sigma_{dc}$ , which is the  $\omega \rightarrow 0$  limit of  $\sigma(\omega)$ , with  $\sigma_0 = \frac{\pi e^2}{\hbar}$  in 2D. (v) Spectral function,  $A(\mathbf{k}, \omega) = -(1/\pi) \text{Im} G(\mathbf{k}, \omega)$  where,  $G(\mathbf{k}, \omega) =$

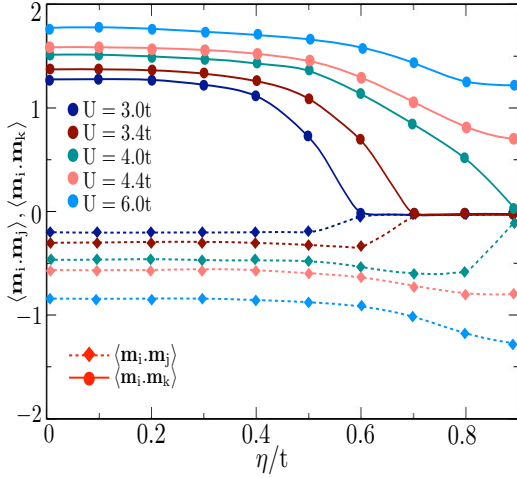


FIG. 2. Strain dependence of the NN ( $\langle \mathbf{m}_i \cdot \mathbf{m}_j \rangle$ ) and the NNN ( $\langle \mathbf{m}_i \cdot \mathbf{m}_k \rangle$ ) correlations at selected interactions, at  $T = 0.01t$ . A positive sign of the magnitude indicates the FM correlation while the AF correlation is characterized by the negative sign.

$\lim_{\delta \rightarrow 0} G(\mathbf{k}, i\omega_n)_{i\omega_n \rightarrow \omega + i\delta}$ .  $G(\mathbf{k}, i\omega_n)$  is the imaginary frequency transform of  $\langle c_{\mathbf{k}}(\tau)c_{\mathbf{k}}(0)^\dagger \rangle$ . The results presented in this paper corresponds to a system size of  $3 \times L^2$ , with  $L = 18$  unless specified otherwise.

### III. LOW TEMPERATURE REGIME

We analyze our results by classifying them in terms of the temperature regimes. We consider  $T \sim 0.01t$ , as the representative of the low temperature regime of the system. The thermal regime ( $T > 0.01t$ ) is analyzed across different temperature cross sections. Note that Mermin-Wagner theorem restricts long range ordering in 2D for  $T > 0$  and the thermodynamic phases that we discuss in this paper are in fact (quasi) long range ordered. Further, the thermal phase transitions discussed herein are essentially Berezinskii-Kosterlitz-Thouless (BKT) transitions<sup>61</sup>. The associated vortex-antivortex formations are however not observable in a finite sized system.

*Magnetic correlations and thermodynamic phases:* We begin the discussion of the low temperature phases with the magnetic correlations across the  $U - \eta$  plane. The static magnetic structure factor  $S(\mathbf{q})$  is shown in Fig.1. The real space correlation function  $\langle \mathbf{m}_i \cdot \mathbf{m}_j \rangle$ , corresponding to the nearest neighbor (NN) antiferromagnetic (AF) and  $\langle \mathbf{m}_i \cdot \mathbf{m}_k \rangle$  corresponding to the next nearest neighbor (NNN) ferromagnetic (FM) correlations, are shown in Fig.2. Across the range of interactions the low strain regime hosts a (quasi) long range magnetic order, dominated by the FM correlations, with subdominant contribution from the AF correlations. Quasi long range AF correlations begin to dominate for  $\eta \gtrsim 0.5t$  depending on the interaction strength ( $U/t$ ), giving rise to a  $\sqrt{3} \times \sqrt{3}$  ordered precursor Coulomb phase<sup>54</sup> at intermediate coupling. A Coulomb phase is realized close to the Kagome limit of  $\eta = t$  at strong cou-

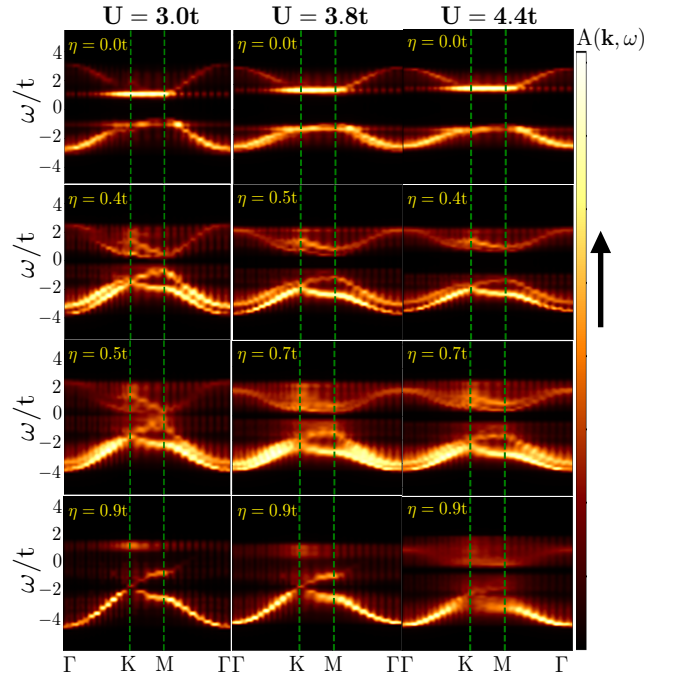


FIG. 3. Spectral function ( $A(\mathbf{k}, \omega)$ ) maps at  $T = 0.01t$  and selected  $U - \eta$  cross sections showing the band structure reconstruction across the Lieb/Kagome interconversion.

pling, quantified in terms of the  $\sqrt{3} \times \sqrt{3}$  order along with the pinch points in the  $S(\mathbf{q})$  maps, which are salient to geometric frustrations<sup>62-68</sup>.

*Electronic band structure:* Fig.3 shows the spectral function ( $A(\mathbf{k}, \omega)$ ) maps at selected  $U - \eta$  cross sections, at  $T = 0.01t$ . The non interacting Lieb lattice ( $\eta = 0.0$ ) is characterized by a flat band at the Fermi level and two dispersive bands which touches the flat band at the  $M$ -point<sup>36,69</sup>. Interaction, as observed from Fig.3, opens up an insulating Mott gap at the Fermi level, with the underlying magnetic phase being dominated by FM correlations. We demarcate this phase as the ferromagnetic insulator (FM-I). The dispersive bands, broadened due to interaction now overlaps the flat band along the  $K - M$  trajectory.

Applied strain has three-fold effect on the electronic band structure: (i) the overall spectrum shifts in energy, (ii) the dispersive bands undergo reconstruction, gives rise to emergent van Hove singularities and opens up topological gaps w. r. t. the flat band and (iii) a gapless spectra is realized at intermediate interactions and strain, indicating the collapse of the insulating (FM-I) phase. At strong interactions, the single particle spectrum is largely gapped across the  $\eta/t$  regime.

Across the range of interactions the large strain regime of  $\eta = 0.9t$  hosts a dominant high energy flat band, akin to the Kagome band structure. Interaction shifts this high energy flat band closer to the Fermi level as compared to the non interacting Kagome lattice where the flat band is at  $\omega \sim 2t$ . This interaction controlled proximity of the flat band to the Fermi level brings forth intriguing transport signatures quantifying

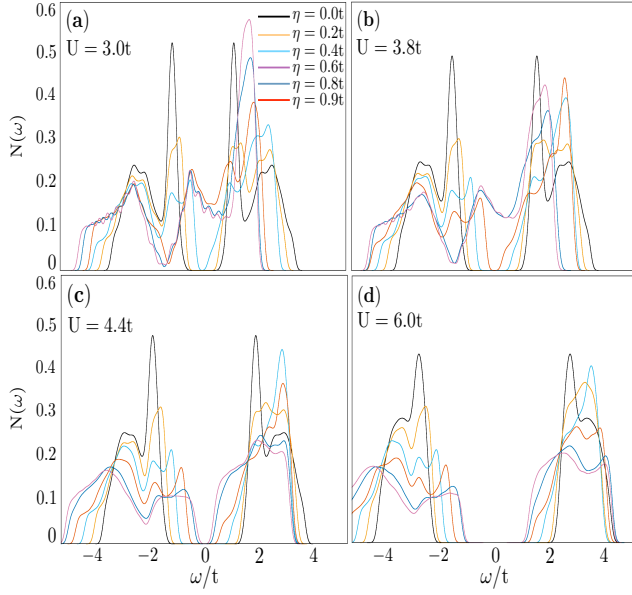


FIG. 4. Single particle DOS ( $N(\omega)$ ) as a function of  $\eta$  at selected interactions representative of: (a) weak ( $U = 3.0t$ ), (b-c) intermediate ( $U = 3.8t$ ,  $U = 4.4t$ ) and (d) strong ( $U = 6.0t$ ) coupling regimes, highlighting the strain controlled gap-gapless transition.

flat band induced dynamic localization of the single particle states<sup>54,55,70,71</sup>.

*Single particle DOS:* Strain tuning of the low temperature single particle DOS at selected interactions is shown in Fig. 4. The FM-I in the weak strain regime is characterized by a robust spectral gap at the Fermi level. Applied strain leads to the progressive suppression this gap such that, in the weak coupling regime a gapless, magnetically disordered state obtains corresponding to a paramagnetic metal (PM-M) (Fig. 4(a)). At intermediate coupling (Fig. 4(b)) the single particle DOS undergoes pronounced and progressive depletion of the spectral weight at  $\omega \approx -1t$  and a gapless spectra at the Fermi level, corresponding to a ferromagnetic metal (FM-M) or an antiferromagnetic metal (AF-M), depending on the choice of  $\eta/t$ . The single particle spectra at the strong coupling, represented by  $U = 4.4t$  (Fig. 4(c)) and  $U = 6.0t$  (Fig. 4(d)) is gapped across the applied strain with the FM-I at weak and intermediate strain giving way to an AF Mott insulator (AF-MI) at large strain, accompanied by an underlying Coulomb phase.

*Optical transport:* The breakdown of the Fermi liquid description of strongly correlated quantum materials is quantified based on the optical absorption spectra. Measurement of low frequency behavior of the optical conductivity ( $\sigma(\omega)$ ) provides unambiguous signatures of the NFL physics in various classes of materials with strong electronic correlations. Prominent examples include, organic molecular charge transfer salt  $\kappa$ -[(BEDT-STF)<sub>x</sub>(BEDT-TTF)<sub>1-x</sub>]<sub>2</sub>Cu<sub>2</sub>(CN)<sub>3</sub><sup>72</sup>, organic Mott insulator  $\kappa$ -(ET)<sub>2</sub>Cu[N(CN)<sub>2</sub>]Cl<sup>73</sup>, 2D transition metal dichalcogenide (TMD) 1T-TaS<sub>2</sub><sup>74</sup>, TMD heterostructure such as, MoTe<sub>2</sub>/WSe<sub>2</sub> Moire superlattices<sup>75</sup>, twisted bilayer WSe<sub>2</sub><sup>76</sup> and more recently Kagome metals such as, Ni<sub>3</sub>In<sup>70</sup>,

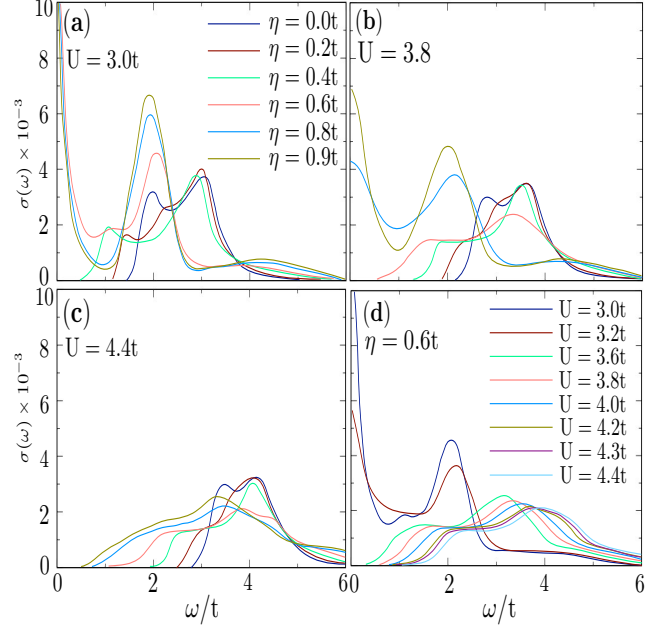


FIG. 5. (a)-(c): Strain dependence of the optical conductivity ( $\sigma(\omega)$ ) at selected interactions, showing the NFL signatures in terms of the DDP and the intermediate frequency polaronic peak. (d) Variation of  $\sigma(\omega)$  with interaction at the selected strain of  $\eta = 0.6t$ .

CsV<sub>3</sub>Sb<sub>3</sub><sup>77</sup> etc. Recent results on the low frequency behavior of  $\sigma(\omega)$  in the large strain regime at  $U \sim t$  revealed a transiently localized insulating phase with *variable* optical conductivity scaling exponent ( $\sigma(\omega) \propto 1/\omega^\gamma$ )<sup>55</sup>. This gapless phase fails to establish any quasi long range magnetic correlation and is typified as a paramagnetic flat band induced insulator (PM-FI). The PM-FI phase is weakly localized and is characterized by a small but finite Inverse Participation Ratio at the Fermi level,  $IPR(\omega = 0)$ , in the thermodynamic limit. It was argued that the local moments originating from the flat electronic bands aid in to localize the fermions at and close to the Fermi level, hence the name<sup>54,55</sup>. The inferences drawn based on the numerical calculations align well with the observations made based on the electrical transport measurements on Kagome metal Ni<sub>3</sub>In, exhibiting pronounced NFL signatures<sup>70</sup>.

The deviation from the conventional  $\sigma(\omega) \propto 1/\omega^2$  dependence results in a finite frequency displaced Drude peak (DDP), a salient feature of the NFL physics<sup>58-60,78-85</sup>. Evidence of the NFL phase can further be observed from the intermediate frequency polaronic peak in  $\sigma(\omega)$ , arising out of the strong correlation between the fermions and the bosonic fields<sup>58-60,86</sup>.

Fig. 5(a-c) shows the strain dependence of  $\sigma(\omega)$  at selected interactions. The optical spectra in the FM-I phase is trivially gapped irrespective of the choice of  $U/t$ . However, in the regime of large  $\eta$  there is finite low frequency spectral weight, in agreement with our observations on the spectral function and the single particle DOS. At  $U = 3.0t$  (Fig. 5(a)) and  $3.8t$  (Fig. 5(b)), for  $\eta \gtrsim 0.5t$  and  $\eta \gtrsim 0.7t$ , respectively,

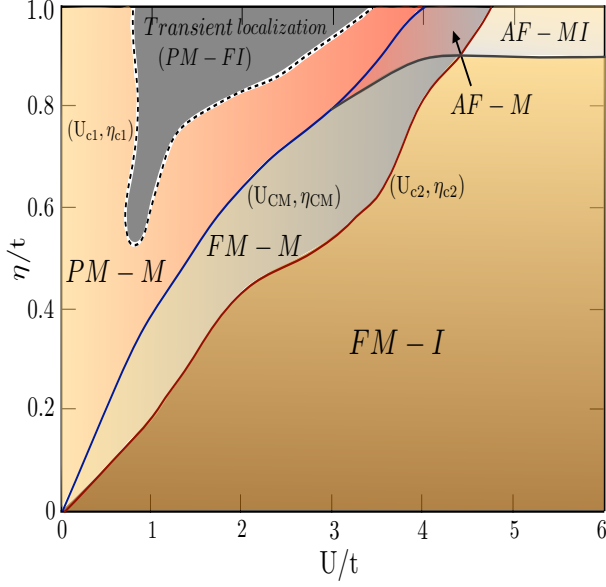


FIG. 6. Phase diagram in the  $U - \eta$  plane, at  $T = 0.01t$  showing the thermodynamic phases: (i) ferromagnetic insulator (FM-I), (ii) ferromagnetic metal (FM-M), (iii) paramagnetic metal (PM-M), (iv) paramagnetic (weak) transiently localized flat band insulator (PM-FI), (v) antiferromagnetic metal (AF-M) and (vi) antiferromagnetic Mott insulator (AF-MI). The critical points  $(U_{c1}, \eta_{c1})$  quantifies the crossover between the PM-M and PM-FI phases while  $(U_{c2}, \eta_{c2})$  demarcates the metal-insulator transition between the FM-I and FM-M phases as well as between the AF-M and AF-MI phases. The onset of the magnetic correlations is typified by the critical point  $(U_{CM}, \eta_{CM})$ . The dashed line shows interpolated boundary of the (weak) transiently localized phase.

$\sigma(\omega) \propto 1/\omega^\gamma$  as  $\omega \rightarrow 0$  and  $\gamma \neq 2$ . The optical spectra is gapped across the strain tuned transition between the FM-I and AF-MI phases, at  $U = 4.4t$  (Fig.5(c)). Fig.5(d) shows the interaction dependence of  $\sigma(\omega)$  at a representative strain of  $\eta = 0.6t$ . Based on the variable scaling exponent ( $\gamma$ ) of the optical conductivity a transition from a gapless NFL metal at weak coupling to a gapped insulator at strong coupling could be ascertained.

*Phase diagram:* Based on the aforementioned signatures we now map out the low temperature  $U - \eta$  phase diagram, at  $T = 0.01t$ , in Fig.6. The thermodynamic phases are demarcated based on the magnetic correlations and the single particle DOS. The metal-insulator transition and/or crossover scales are determined based on the low temperature behavior of the longitudinal resistivity ( $\rho_{xx}$ ) (discussed in the next section). Fig.6 shows that the weak  $\eta/t$  regime is FM-I across the range of interactions, dominated by NNN FM correlations with strongly suppressed single particle transport. The FM-I encompasses a large part of the  $U - \eta$  plane giving way to a NFL metal at intermediate  $U - \eta$  and to a dominantly AF phase at large  $U - \eta$ . The metallic phase at intermediate  $U - \eta$  can further be classified into the ferromagnetically correlated metal (FM-M) and the disordered paramagnetic metal (PM-

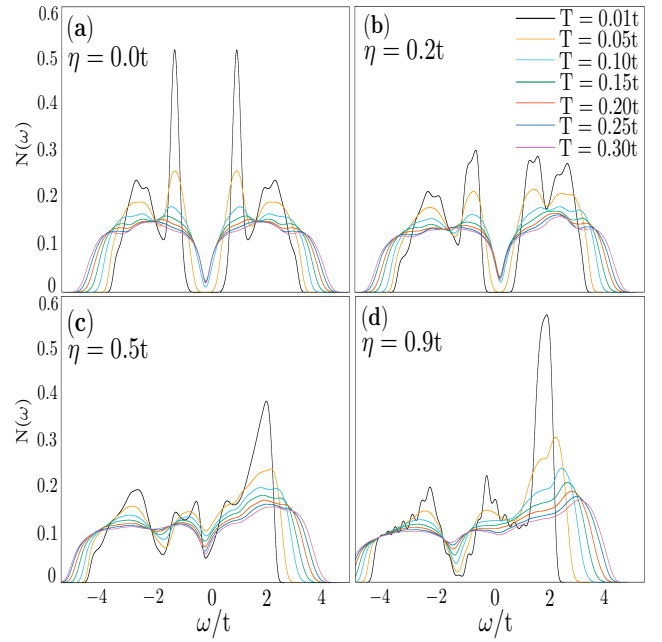


FIG. 7. Thermal evolution of the single particle DOS at  $U = 3.0t$  showing the thermal fluctuations induced accumulation of spectral weight and the origin of gapless phase for selected: (a)  $\eta = 0.0t$  (b)  $\eta = 0.2t$ , (c)  $\eta = 0.5t$  and (d)  $\eta = 0.9t$ .

M). These phases are by definition gapless and are NFL with pronounced deviation from the Fermi liquid description.

The thermodynamic phase boundaries are associated with critical interactions and strains,  $(U_{c1}, \eta_{c1})$ ,  $(U_{CM}, \eta_{CM})$  and  $(U_{c2}, \eta_{c2})$  quantifying: (i) a metal-insulator crossover between the weak transiently localized PM-FI and PM-M at  $(U_{c1}, \eta_{c1})$ , across which no quantum symmetry breaking takes place and the system undergoes a gradual suppression of the single particle charge transport, (ii) a magnetic order-disorder transition across  $(U_{CM}, \eta_{CM})$  between the PM-M/FM-M and PM-M/AF-M phases at the intermediate and large  $U/t, \eta/t$ , respectively, and (iii) a metal-insulator transition between the FM-I/FM-M at intermediate  $U, \eta/t$  and between AF-MI/AF-M at large  $U/t, \eta/t$ , respectively, across  $(U_{c2}, \eta_{c2})$ . Finally, an insulator-insulator magnetic transition takes place at the large  $\eta/t$  deep in the strong coupling regime between the FM-I and the AF-MI phases.

#### IV. THERMAL PHASES AND SCALES

With the low temperature phases in the  $U - \eta$  plane in place we now select particular cross sections representative of the various phases of Fig.6, to highlight the impact of thermal fluctuations on the thermodynamic phases and the associated thermal scales. Our analyses is based once again on the spectroscopic, transport and thermodynamic signatures of the system.

*Single particle DOS:* Fig.7(a-d) shows the thermal evolution of the single particle DOS at  $U = 3.0t$  for the selected

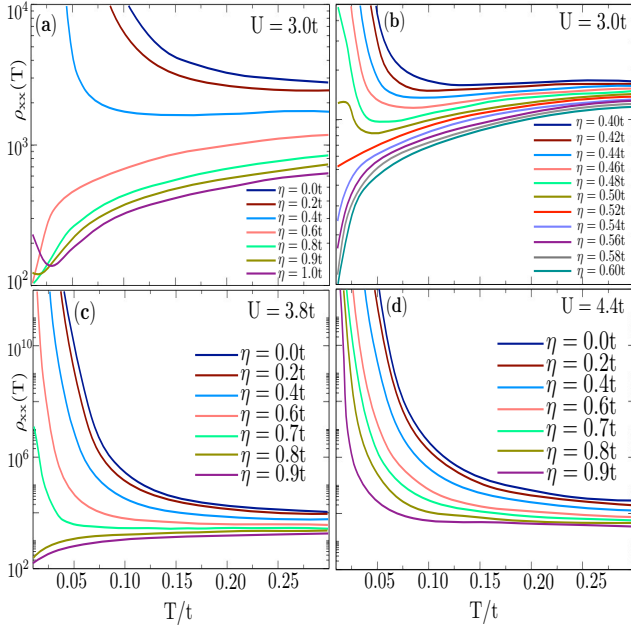


FIG. 8. (a-d) Temperature dependence of the longitudinal resistivity  $\rho_{xx}(T)$  at selected  $U - \eta$  cross sections demarcating the metal and the insulator phases based on the sign change of  $d\rho_{xx}/dT$ , as  $T \rightarrow 0$ . A  $d\rho_{xx}/dT > 0$  signifies a metallic phase while an insulating phase is typified by  $d\rho_{xx}/dT < 0$ .

$\eta = 0.0t$  (Fig. 7(a)),  $\eta = 0.2t$  (Fig. 7(b)),  $\eta = 0.5t$  (Fig. 7(c)) and  $\eta = 0.9t$  (Fig. 7(d)). At and close to the Lieb limit the (quasi) long range magnetic order is signified by the sharp van Hove singularities at the gap edges (Fig. 7(a-b)). Thermal fluctuations induced randomness of the local moments destabilize the (quasi) long range order and gives way to short range magnetic correlations. The corresponding single particle DOS is rendered gapless via the accumulation of spectral weight at the Fermi level that leads to the eventual closure of the gap. Apart from the large transfer of spectral weights away from the Fermi level the single particle DOS is largely immune to temperature.

The NFL metal at the intermediate strain (Fig. 7(c)), is essentially gapless with large spectral weight at the Fermi level at all temperatures. The broad high energy peak at  $\omega \sim 2t$  signifies the strain tuned band structure reconstruction as the system moves away from the Lieb and towards the Kagome limit. For  $T \gtrsim 0.05t$  the spectral weight begins to deplete giving rise to a dip at the Fermi level, an observation akin to the pseudogap formation in superconductors and correlated metals at finite temperatures. This suggests that even though the magnetic local moments fail to establish a (quasi) long range order, their short range correlations dominate the finite temperature regime at this  $U - \eta$  cross section.

In the large strain regime (Fig. 7(d)), the single particle DOS at the Fermi level is largely featureless with a pronounced high energy peak at  $\omega \sim 2t$  reminiscent of the Kagome limit. Thermal fluctuations progressively suppress this high energy peak as the electronic band structure is de-

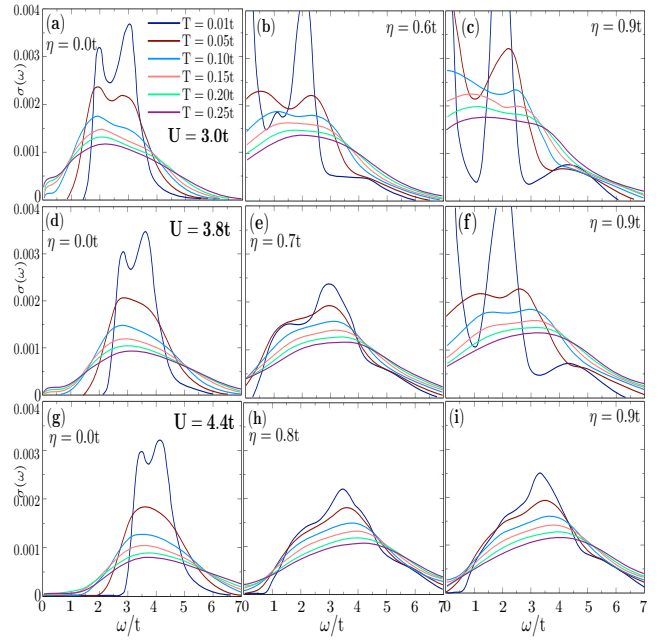


FIG. 9. (a-i): Thermal evolution of  $\sigma(\omega)$  at selected  $U - \eta$  cross sections showing the NFL metal and its thermal fluctuations induced crossover to the bad metal phase via the loss of the DDP and the polaronic peak.

stroyed via thermal broadening. The single particle DOS shown in Fig. 7(a-d) are generic for the larger part of the  $U - \eta$  plane. The strong coupling large strain AF-MI phase is quantified by a robust spectral gap at the Fermi level which remains largely immune to temperature. The weak transiently localized PM-FI phase is essentially gapless across the temperature regime<sup>55</sup>.

*Longitudinal resistivity:* One of the primary indicators of the Fermi liquid description of a metal and the deviations thereof is the low temperature behavior of its longitudinal resistivity ( $\rho_{xx}$ ). For a conventional metal obeying the Fermi liquid description the electrical conductivity scales as the quasi-particle lifetime  $\tau$  and the corresponding resistivity behaves as,  $\rho_{xx} \propto T^2$ . This relation is often found to be violated in case of materials with strong electronic correlations wherein the Fermi surface is redundant and the quasiparticle lifetime is cut short<sup>58,72,73,75-77,84,87</sup>. In Fig. 8 we present  $\rho_{xx}(T)$  as a function of the applied strain  $\eta/t$  at selected interactions. The distinction between the metallic and insulating phases are made based on the change in the sign of  $d\rho_{xx}/dT$  as  $T \rightarrow 0$ , such that,  $d\rho_{xx}/dT > 0$  signifies a metallic phase while an insulating phase is typified by  $d\rho_{xx}/dT < 0$ . At  $U = 3.0t$ , (Fig. 8(a)-(b)) across the Lieb/Kagome interconversion the metal-insulator transition between the FM-I and NFL metal takes place at  $\eta \approx 0.52t$ . In the large strain regime  $\eta \gtrsim 0.8t$ , the observed  $d\rho_{xx}/dT < 0$  indicates the re-entrant crossover of the metal to the weakly localized PM-FI phase.

At  $U = 3.8t$  the metal-insulator transition between the FM-I and NFL metal (FM-M and AF-M) takes place at  $\eta \gtrsim 0.8t$ , as shown in Fig. 8(c). Finally, Fig. 8(d) corresponds to  $U = 4.4t$

representative of a regime which lacks any metal-insulator transition. The system is a FM-I at weak and intermediate strain ( $0 < \eta \lesssim 0.7t$ ) and undergoes transition to a AF-MI phase in the large strain regime (Fig.8(d)).

Across the  $U - \eta$  plane,  $\rho_{xx}(T)$  as  $T \rightarrow 0$  exhibits pronounced deviation from the  $\rho_{xx} \propto T^2$  behavior, attesting that the underlying phase is a NFL<sup>58,72,73,75-77,84,87</sup>. In the weak coupling regime ( $U = t$ ) a  $\eta$ -dependent variable resistivity scaling exponent  $\rho_{xx} = \rho(0) + AT^\alpha$ , was recently reported, such that, at large strain  $\alpha \sim 1.3, 1.5, 1.9$  for  $\eta = 0.75, 0.85, 0.95$ , respectively<sup>55</sup>. On the other hand the metallic regime at the intermediate strain  $0.4 \lesssim \eta < 0.7$  for  $U = t$  exhibits a *linear*-T ( $\alpha = 1$ ) dependence of  $\rho_{xx}(T)$ . The variable resistivity scaling exponent is considered to be a hallmark of NFL physics. Such variable scaling exponents have been experimentally observed in heavy fermion materials<sup>88-91</sup>, disorder-controlled metal-Mott insulator transitions<sup>92</sup>, Anderson insulators with disorder-localized single particle states<sup>93</sup> and very recently in Kagome metal CeRhSn<sup>94</sup>. Recent transport measurements on the Kagome metal Ni<sub>3</sub>In revealed similar NFL signatures, which were attributed to be arising from a flat band induced localization of the itinerant fermions<sup>70,71</sup>.

*Crossover to bad metal:* The breakdown of the Fermi liquid description is further analyzed based on the optical transport signatures viz. optical conductivity ( $\sigma(\omega)$ ). The thermal evolution of the same is presented in Fig.9 across selected  $U - \eta$  cross sections. The low temperature regime exhibits the suppression of the single particle transport at low frequencies and a DDP with a variable scaling exponent  $\gamma$  such that,  $\sigma(\omega) \propto 1/\omega^\gamma$  with  $\gamma \neq 2$ . Thermal fluctuations of the local moments lead to the crossover of the NFL to the bad metal phase.

The intermediate frequency optical spectra is characterized by a polaronic peak arising due to the strong correlation between the bosonic background and the itinerant fermions. Thermal fluctuations induced crossover of the NFL to the bad metal phase is quantified in terms of the melting of the polaronic peak, which defines the thermal scale  $T_{IRM}(\eta)$  corresponding to the Ioffe-Regel-Mott temperature<sup>80,81</sup>. The NFL-bad metal crossover is quantified in terms of the following criteria: (i)  $A(T) \lesssim A(T_0)/3$  and (ii)  $\Gamma_{norm} = \Gamma/\omega_{peak} \geq 1$ , where,  $A(T)$ ,  $\Gamma$  and  $\omega_{peak}$  correspond to the amplitude ( $A(T_0)$  is the amplitude at  $T = 0.01t$ ), the full width at half maxima (FWHM) and the polaronic peak frequency, respectively. These quantifiers are determined by fitting the intermediate frequency optical spectra to a Lorentzian,  $g(x) = A(T)/(1 + ((x - \omega_{peak})/\Gamma)^2)$ <sup>55</sup>. Based on these criteria, one obtains for  $U = 3.0t$ ,  $\eta = 0.6t$  the  $T_{IRM} \sim 0.1t$  while for  $\eta = 0.9t$ ,  $T_{IRM} \sim 0.15t$ .

The applied strain stabilizes the NFL phase against thermal fluctuations. The observation is generic across the  $U - \eta$  plane. Note that the NFL to bad metal crossover has been reported in a wide class of materials such as, 2D TMD<sup>74-76</sup>, organic charge transfer salts<sup>72,73</sup>, rare-earth nickelates<sup>95</sup> and more recently Kagome metals<sup>77</sup>; with doping, temperature and electrical gating serving as the suitable control parameters.

*Static magnetic structure factor:* In order to understand the

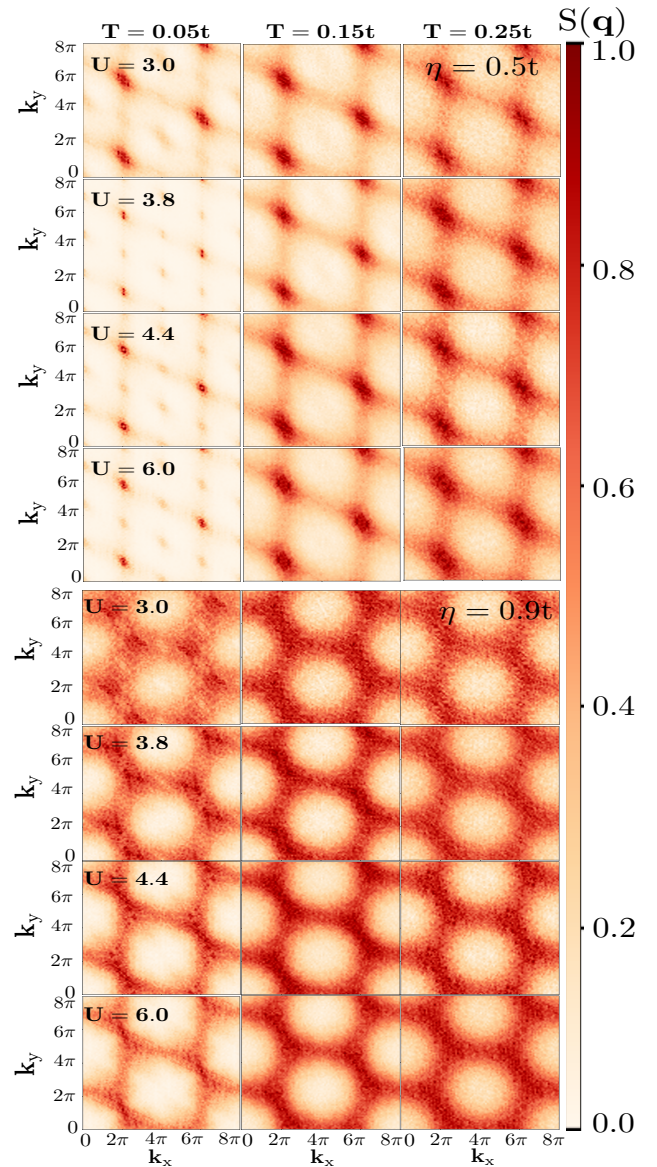


FIG. 10. Thermal evolution of the static magnetic structure factor ( $S(\mathbf{q})$ ) at  $\eta = 0.5t$  (intermediate strain) and  $\eta = 0.9t$  (large strain) for selected interactions, showing the progressive loss of magnetic correlations due to the thermal fluctuations induced disordering of the local magnetic moments. For each choice of  $\eta$ , temperature varies along the row while  $U/t$  varies along the column.

fate of the magnetic correlations across the  $U - \eta - T$  space we track the corresponding  $S(\mathbf{q})$  as shown in Fig.10 at the selected strain of  $\eta = 0.5t$  and  $0.9t$ . At  $\eta = 0.5t$  the magnetic correlations across the  $U \gtrsim 3t$  regime (along the column) is largely the same at low temperatures with  $S(\mathbf{q})$  exhibiting coexisting (quasi) long range magnetic order dominated by FM correlations with a finite but subdominant AF component. Thermal fluctuations (along the row) broaden the  $S(\mathbf{q})$  peaks allowing them to overlap, with the high temperature phase merely mapping out the non interacting Brillouin

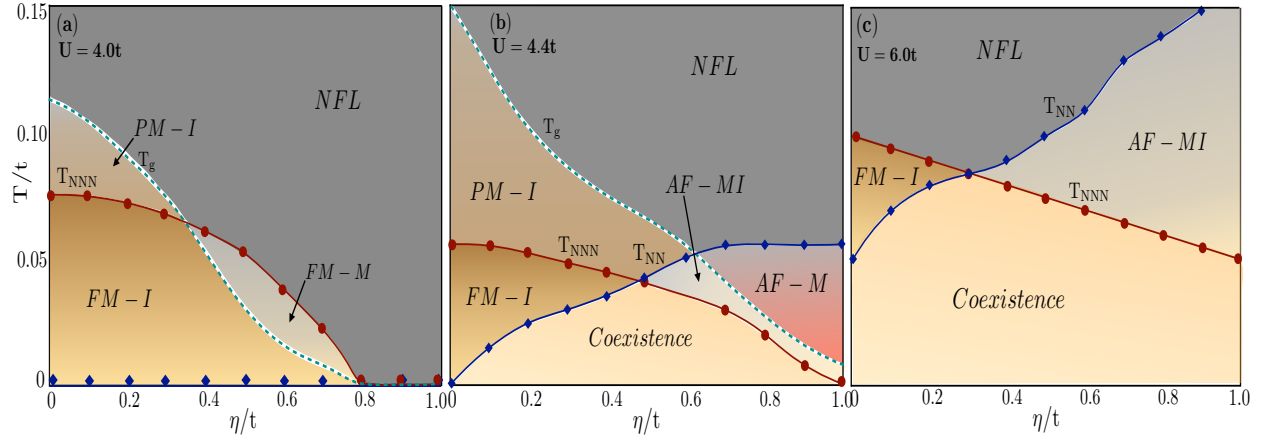


FIG. 11. Thermal phase diagram in the  $\eta - T$  plane at selected interactions representing various thermodynamic phases. The thermal transition scales  $T_{NN}$  and  $T_{NNN}$  correspond to the thermal fluctuations induced loss of the NN and the NNN magnetic correlations, while  $T_g$  represents the crossover thermal scale between the gapped and gapless phases (see text).

zone of the underlying lattice.

At  $\eta = 0.9t$ , the system at low temperatures undergo cross over from one magnetic order to another as the interaction is tuned. The  $\eta = 0.9t, U = 3t, T = 0.05t$  cross section shows the reminiscent of the precursor Coulomb phase. Increasing interaction leads to the Coulomb phase. Thermal fluctuation results in the disordering of the (quasi) long range magnetic correlations, broadens the  $S(\mathbf{q})$  peaks and eventually maps out the Brillouin zone akin to that of the Kagome lattice. The magnetic correlations remain largely immune to the interactions for  $U \geq 4.4t$  in the large strain limit, while at  $U = 3.8t$ , thermal fluctuations destroy the precursor Coulomb phase to give rise to the magnetically disordered state.

*Thermal phase diagram:* We next elucidate the thermal phases and the associated scales across the  $U - \eta$  plane and distill the corresponding phase diagram in terms of the: (i) temperature dependent NN and the NNN magnetic correlations and (ii) thermal evolution of the single particle DOS. The crossover between the gapped and gapless phases is typified by the single particle DOS in terms of the thermal scale  $T_g$ . We select three particular  $U$ 's viz.  $U = 4.0t, U = 4.4t$  and  $U = 6.0t$ , representative of the three different low temperature regimes and present the corresponding finite temperature  $\eta - T$  phase diagram in Fig. 11.

At  $U = 4.0t$  (Fig. 11(a)), the thermal transition scale  $T_{NNN}$  demarcates the FM correlated phase from the PM phases. The AF correlations are however strongly suppressed across the regime of strain. Over the regime  $0 < \eta \lesssim 0.8t$  the low temperature phase is FM-I. Thermal fluctuations though destroys the magnetic correlations at  $T_{NNN}$ , don't close the single particle spectral gap at the Fermi level. This brings forth a magnetically disordered gapped insulating phase PM-I over the temperature regime  $0.07t < T \lesssim 0.11t$ , demarcated by the thermal scale  $T_g$ . We understand this phase as follows: while thermal fluctuations destroy the angular correlations between the local moments  $\mathbf{m}_i$  and randomizes them, the strong coupling ensures a large  $|\mathbf{m}_i|$  which couldn't get

suppressed over this narrow temperature regime. The PM-I phase can therefore be envisaged as a regime of randomly oriented large local moments which though fails to order magnetically, don't close the excitation gap at the Fermi level. The gap closure takes place for  $T \geq T_g$  leading to a NFL metal with short range magnetic correlations between the suppressed local magnetic moments. Over a narrow regime of strain  $0.6t < \eta \lesssim 0.8t$ , a finite temperature FM-M phase obtains, quantified by  $T_g < T \lesssim T_{NNN}$ , corresponding to a FM correlated gapless state.

The  $U = 4.4t$  (Fig. 11(b)) cross section comprises of a FM-I phase close to the Lieb limit, over the temperature regime  $0 < T \lesssim 0.04t$ , with a dominant  $T_{NNN}$  scale. Thermal fluctuations promote the AF correlations while simultaneously suppressing the FM order, giving rise to a finite temperature coexistence phase with competing  $T_{NNN}$  and  $T_{NN}$  scales. While  $T_{NNN}$  and the corresponding FM correlations are strongly suppressed at  $\eta \sim 0.8t$ , the AF correlations are dominant over this regime and  $T_{NN}$  saturates to a finite value at large strain. This finite temperature AF phase can further be demarcated into AF-M and AF-MI regimes based on  $T_g$  determined from the single particle spectra. Further, a significant finite temperature PM-I regime is mapped out by  $T_g$  at weak and intermediate strain, quantified by large randomly oriented local moments with a finite single particle spectral gap at the Fermi level. The  $T > T_g$  regime essentially corresponds to a NFL metal.

The low temperature regime at the strong coupling with  $U = 6t$  (Fig. 11(c)) is characterized by a FM-I for  $0 < \eta \lesssim 0.9t$  and a AF-MI for  $\eta \geq 0.9t$ . Thermal fluctuations significantly enhances the AF correlations leading to a large  $T_{NN}$  scale that increases with  $\eta$ , at the same time weakly suppressing the  $T_{NNN}$  scale corresponding to the FM correlations. A large part of the  $\eta - T$  plane therefore hosts a coexistence phase with competing FM and AF correlations. The weak strain regime continues to be a FM-I at finite temperatures while the large strain regime hosts a finite temperature AF-MI phase. The single particle spectra is gapped across the  $\eta - T$  plane

corresponding to an insulator. The regime of  $T \geq T_{NNN}$  and  $T \geq T_{NV}$  is a NFL metal with finite spectral weight at the Fermi level in the single particle spectra. Note that at higher temperature a thermal crossover scale  $T_{IRM}$  quantifies the crossover from the NFL to the bad metal phase independent of  $U/t$  and  $\eta/t$ .

## V. DISCUSSION AND CONCLUSION

Fig.6 and Fig.11 constitutes the primary results of this work wherein we have mapped out the low temperature phases and thermal scales in the  $U - \eta$ -plane. Our results on the thermodynamic, spectroscopic and transport properties have brought forth the applied strain as a suitable tuning parameter for the Lieb/Kagome interconversion; a cleaner alternative to disorder and chemical doping. The straintronics protocol discussed in this paper is generic and should be applicable to other line-graph lattices as well.

The calculations are carried out using the SPA Monte Carlo simulation based on adiabatic approximation wherein the fast moving fermions are subjected to the spatially inhomogeneous background of slow thermal bosons. SPA can suitably capture the temperature regime of  $T > T_{FL}$ . This is particularly important in case of geometrically frustrated systems such as, Kagome metal whose low temperature physics evades the standard numerical tools owing to severe fermion sign problem and system size restrictions.

The NFL metal observed both at the low and finite temperatures is characterized by the deviation of the transport signatures from the Fermi liquid description. Of particular importance is the strain dependent variable scaling exponents of the low temperature longitudinal resistivity ( $\rho_{xx}(T) \propto T^\alpha$ ) and low frequency optical conductivity ( $\sigma(\omega) \propto 1/\omega^\gamma$ ). Similar observations of variable transport scaling exponents have been made in case of heavy fermion systems<sup>88-91</sup>, disorder induced phase transition<sup>92,93</sup> and more recently in Kagome metals<sup>94</sup>, thus establishing the fermionic localization by a fluctuating

random background of slow bosons as a plausible explanation for the breakdown of the Fermi liquid description.

It must be noted that the transient localization observed in the weak coupling regime of the system discussed in the preceding sections is a natural outcome of fermions interacting with the thermal bosons<sup>58-60,86</sup>. This PM-FI regime is weakly localized and is therefore prone to system size effects. In 2D, a finite sized system can host a weakly localized phase at weak coupling when  $L < \xi$  (where,  $\xi$  is the localization length)<sup>96</sup>. Across the Lieb/Kagome interconversion, the (weak) transiently localized regime constitutes a stable low temperature phase in the  $U - \eta - T$  space, for system sizes accessible within reasonable computation cost<sup>55</sup>. The key drawback of the adiabatic approximation of SPA is its failure to capture the  $T < T_{FL}$  regime, where the translation invariance is restored and the system behaves as a conventional Fermi liquid, as experimentally observed in several classes of strongly correlated quantum materials<sup>72,73,75-77</sup>.

One of the suitable platforms to realize the strain controlled metal-insulator transition discussed in this work is MOF. Phenomena such as, charge transfer, gate tuning and strain engineering are shown to reveal strong electronic correlation effects in MOF<sup>30,31,40,97-101</sup>. Unconventional superconductivity<sup>99</sup>, exchange correlation induced ferromagnetism<sup>98</sup> and recently gate controlled Mott insulator-metal transitions<sup>97</sup> are reported in MOFs, making them a suitable and promising platform to realize straintronics across the Lieb/Kagome interconversion.

## VI. ACKNOWLEDGEMENTS

MK would like to acknowledge the use of the high performance computing facility (AQUA) at the Indian Institute of Technology, Madras, India. MK acknowledges the support from the Department of Science and Technology, Govt. of India through the grant CRG/2023/002593.

\* [madhuparna.k@gmail.com](mailto:madhuparna.k@gmail.com)

<sup>1</sup> Satoru Nakatsuji, Naoki Kiyohara, and Tomoya Higo, "Large anomalous hall effect in a non-collinear antiferromagnet at room temperature," *Nature* **527**, 212 (2015).

<sup>2</sup> Ajaya K. Nayak, Julia Erika Fischer, Yan Sun, Binghai Yan, Julie Karel, Alexander C. Komarek, Chandra Shekhar, Nitesh Kumar, Walter Schnelle, Jürgen Kübler, Claudia Felser, and Stuart S. P. Parkin, "Large anomalous hall effect driven by a nonvanishing berry curvature in the noncollinear antiferromagnet mn<sub>3</sub>ge," *Science Advances* **2**, e1501870 (2016).

<sup>3</sup> K. Kuroda, T. Tomita, M. T. Suzuki, C. Bareille, A. A. Nugroho, P. Goswami, M. Ochi, M. Ikhlal, M. Nakayama, S. Akebi, R. Noguchi, R. Ishii, N. Inami, K. Ono, H. Kumigashira, A. Varykhalov, T. Muro, T. Koretsune, R. Arita, S. Shin, Takeshi Kondo, and S. Nakatsuji, "Evidence for magnetic weyl fermions in a correlated metal," *Nature Materials* **16**, 1090 (2017).

<sup>4</sup> Motoi Kimata, Hua Chen, Kouta Kondou, Satoshi Sugimoto, Prasanta K. Muduli, Muhammad Ikhlal, Yasutomo Omori,

Takahiro Tomita, Allan. H. MacDonald, Satoru Nakatsuji, and Yoshichika Otani, "Magnetic and magnetic inverse spin hall effects in a non-collinear antiferromagnet," *Nature* **565**, 627 (2019).

<sup>5</sup> Xiaokang Li, Clément Collignon, Liangcai Xu, Huakun Zuo, Antonella Cavanna, Ulf Gennser, Dominique Mailly, Benoît Fauqué, Leon Balents, Zengwei Zhu, and Kamran Behnia, "Chiral domain walls of mn<sub>3</sub>sn and their memory," *Nature Communications* **10**, 3021 (2019).

<sup>6</sup> Christoph Wuttke, Federico Caglieris, Steffen Sykora, Francesco Scaravaggi, Anja U. B. Wolter, Kaustuv Manna, Vicky Süss, Chandra Shekhar, Claudia Felser, Bernd Büchner, and Christian Hess, "Berry curvature unravelled by the anomalous nernst effect in mn<sub>3</sub>ge," *Phys. Rev. B* **100**, 085111 (2019).

<sup>7</sup> L A Fenner, A A Dee, and A S Wills, "Non-collinearity and spin frustration in the itinerant kagome ferromagnet fe<sub>3</sub>sn<sub>2</sub>," *Journal of Physics: Condensed Matter* **21**, 452202 (2009).

- <sup>8</sup> Zhipeng Hou, Weijun Ren, Bei Ding, Guizhou Xu, Yue Wang, Bing Yang, Qiang Zhang, Ying Zhang, Enke Liu, Feng Xu, Wenhong Wang, Guangheng Wu, Xixiang Zhang, Baogen Shen, and Zhidong Zhang, "Observation of various and spontaneous magnetic skyrmionic bubbles at room temperature in a frustrated kagome magnet with uniaxial magnetic anisotropy," *Advanced Materials* **29**, 1701144 (2017).
- <sup>9</sup> Linda Ye, Mingu Kang, Junwei Liu, Felix von Cube, Christina R. Wicker, Takehito Suzuki, Chris Jozwiak, Aaron Bostwick, Eli Rotenberg, David C. Bell, Liang Fu, Riccardo Comin, and Joseph G. Checkelsky, "Massive dirac fermions in a ferromagnetic kagome metal," *Nature* **555**, 638 (2018).
- <sup>10</sup> Jia-Xin Yin, Songtian S. Zhang, Hang Li, Kun Jiang, Guoqing Chang, Bingjing Zhang, Biao Lian, Cheng Xiang, Ilya Belopolski, Hao Zheng, Tyler A. Cochran, Su-Yang Xu, Guang Bian, Kai Liu, Tay-Rong Chang, Hsin Lin, Zhong-Yi Lu, Ziqiang Wang, Shuang Jia, Wenhong Wang, and M. Zahid Hasan, "Giant and anisotropic many-body spin-orbit tunability in a strongly correlated kagome magnet," *Nature* **562**, 91 (2018).
- <sup>11</sup> Zhiyong Lin, Jin-Ho Choi, Qiang Zhang, Wei Qin, Seho Yi, Pengdong Wang, Lin Li, Yifan Wang, Hui Zhang, Zhe Sun, Laiming Wei, Shengbai Zhang, Tengfei Guo, Qingyou Lu, Jun-Hyung Cho, Changgan Zeng, and Zhenyu Zhang, "Flatbands and emergent ferromagnetic ordering in  $\text{Fe}_3\text{Sn}_2$  kagome lattices," *Phys. Rev. Lett.* **121**, 096401 (2018).
- <sup>12</sup> Hang Li, Bei Ding, Jie Chen, Zefang Li, Zhipeng Hou, Enke Liu, Hongwei Zhang, Xuekui Xi, Guangheng Wu, and Wenhong Wang, "Large topological Hall effect in a geometrically frustrated kagome magnet  $\text{Fe}_3\text{Sn}_2$ ," *Applied Physics Letters* **114**, 192408 (2019).
- <sup>13</sup> Yangmu Li, Qi Wang, Lisa DeBeer-Schmitt, Zurab Guguchia, Ryan D. Desautels, Jia-Xin Yin, Qianheng Du, Weijun Ren, Xinguo Zhao, Zhidong Zhang, Igor A. Zaliznyak, Cedimir Petrovic, Weiguo Yin, M. Zahid Hasan, Hechang Lei, and John M. Tranquada, "Magnetic-field control of topological electronic response near room temperature in correlated kagome magnets," *Phys. Rev. Lett.* **123**, 196604 (2019).
- <sup>14</sup> Hiroaki Tanaka, Yuita Fujisawa, Kenta Kuroda, Ryo Noguchi, Shunsuke Sakuragi, Cédric Bareille, Barnaby Smith, Cephise Cacho, Sung Won Jung, Takayuki Muro, Yoshinori Okada, and Takeshi Kondo, "Three-dimensional electronic structure in ferromagnetic  $\text{Fe}_3\text{Sn}_2$  with breathing kagome bilayers," *Phys. Rev. B* **101**, 161114 (2020).
- <sup>15</sup> Enke Liu, Yan Sun, Nitesh Kumar, Lukas Muechler, Aili Sun, Lin Jiao, Shuo-Ying Yang, Defa Liu, Aiji Liang, Qianan Xu, Johannes Kroder, Vicky Süß, Horst Borrmann, Chandra Shekhar, Zhaosheng Wang, Chuanying Xi, Wenhong Wang, Walter Schnelle, Steffen Wirth, Yulin Chen, Sebastian T. B. Goennenwein, and Claudia Felser, "Giant anomalous hall effect in a ferromagnetic kagome-lattice semimetal," *Nature Physics* **14**, 1125 (2018).
- <sup>16</sup> Qi Wang, Yuanfeng Xu, Rui Lou, Zhonghao Liu, Man Li, Yaobo Huang, Dawei Shen, Hongming Weng, Shancai Wang, and Hechang Lei, "Large intrinsic anomalous hall effect in half-metallic ferromagnet  $\text{Co}_3\text{Sn}_2\text{S}_2$  with magnetic weyl fermions," *Nature Communications* **9**, 3681 (2018).
- <sup>17</sup> Jia-Xin Yin, Songtian S. Zhang, Guoqing Chang, Qi Wang, Stepan S. Tsirkin, Zurab Guguchia, Biao Lian, Huibin Zhou, Kun Jiang, Ilya Belopolski, Nana Shumiya, Daniel Multer, Maksim Litskevich, Tyler A. Cochran, Hsin Lin, Ziqiang Wang, Titus Neupert, Shuang Jia, Hechang Lei, and M. Zahid Hasan, "Negative flat band magnetism in a spin-orbit-coupled correlated kagome magnet," *Nature Physics* **15**, 443 (2019).
- <sup>18</sup> D. F. Liu, A. J. Liang, E. K. Liu, Q. N. Xu, Y. W. Li, C. Chen, D. Pei, W. J. Shi, S. K. Mo, P. Dudin, T. Kim, C. Cacho, G. Li, Y. Sun, L. X. Yang, Z. K. Liu, S. S. P. Parkin, C. Felser, and Y. L. Chen, "Magnetic weyl semimetal phase in a kagomé crystal," *Science* **365**, 1282 (2019).
- <sup>19</sup> Jianlei Shen, Qingqi Zeng, Shen Zhang, Wei Tong, Langsheng Ling, Chuanying Xi, Zhaosheng Wang, Enke Liu, Wenhong Wang, Guangheng Wu, and Baogen Shen, "On the anisotropies of magnetization and electronic transport of magnetic Weyl semimetal  $\text{Co}_3\text{Sn}_2\text{S}_2$ ," *Applied Physics Letters* **115**, 212403 (2019).
- <sup>20</sup> Ella Lachman, Ryan A. Murphy, Nikola Maksimovic, Robert Kealhofer, Shannon Haley, Ross D. McDonald, Jeffrey R. Long, and James G. Analytis, "Exchange biased anomalous hall effect driven by frustration in a magnetic kagome lattice," *Nature Communications* **11**, 560 (2020).
- <sup>21</sup> Sean Howard, Lin Jiao, Zhenyu Wang, Praveen Vir, Chandra Shekhar, Claudia Felser, Taylor Hughes, and Vidya Madhavan, "Observation of linearly dispersive edge modes in a magnetic weyl semimetal  $\text{Co}_3\text{Sn}_2\text{S}_2$ ," (2021), [arXiv:1910.11205 \[cond-mat.mtrl-sci\]](https://arxiv.org/abs/1910.11205).
- <sup>22</sup> S. Nakamura, N. Kabeya, M. Kobayashi, K. Araki, K. Katoh, and A. Ochiai, "Spin trimer formation in the metallic compound  $\text{gd}_3\text{ru}_4\text{al}_{12}$  with a distorted kagome lattice structure," *Phys. Rev. B* **98**, 054410 (2018).
- <sup>23</sup> Takeshi Matsumura, Yusaku Ozono, Shintaro Nakamura, Noriyuki Kabeya, and Akira Ochiai, "Helical ordering of spin trimers in a distorted kagome lattice of  $\text{gd}_3\text{ru}_4\text{al}_{12}$  studied by resonant x-ray diffraction," *Journal of the Physical Society of Japan* **88**, 023704 (2019).
- <sup>24</sup> Hisashi Inoue, Minyong Han, Linda Ye, Takehito Suzuki, and Joseph G. Checkelsky, "Molecular beam epitaxy growth of antiferromagnetic Kagome metal  $\text{FeSn}$ ," *Applied Physics Letters* **115**, 072403 (2019).
- <sup>25</sup> Mingu Kang, Linda Ye, Shiang Fang, Jih-Shih You, Abe Levitan, Minyong Han, Jorge I. Facio, Chris Jozwiak, Aaron Bostwick, Eli Rotenberg, Mun K. Chan, Ross D. McDonald, David Graf, Konstantine Kaznatcheev, Elio Vescovo, David C. Bell, Efthimios Kaxiras, Jeroen van den Brink, Manuel Richter, Madhav Prasad Ghimire, Joseph G. Checkelsky, and Riccardo Comin, "Dirac fermions and flat bands in the ideal kagome metal  $\text{FeSn}$ ," *Nature Materials* **19**, 163 (2019).
- <sup>26</sup> Zhiyong Lin, Chongze Wang, Pengdong Wang, Seho Yi, Lin Li, Qiang Zhang, Yifan Wang, Zhongyi Wang, Hao Huang, Yan Sun, Yaobo Huang, Dawei Shen, Donglai Feng, Zhe Sun, Jun-Hyung Cho, Changgan Zeng, and Zhenyu Zhang, "Dirac fermions in antiferromagnetic  $\text{FeSn}$  kagome lattices with combined space inversion and time-reversal symmetry," *Phys. Rev. B* **102**, 155103 (2020).
- <sup>27</sup> Brian C. Sales, Jiaqiang Yan, William R. Meier, Andrew D. Christianson, Satoshi Okamoto, and Michael A. McGuire, "Electronic, magnetic, and thermodynamic properties of the kagome layer compound  $\text{FeSn}$ ," *Phys. Rev. Mater.* **3**, 114203 (2019).
- <sup>28</sup> Brenden R. Ortiz, Lídia C. Gomes, Jennifer R. Morey, Michal Winiarski, Mitchell Bordelon, John S. Mangum, Iain W. H. Oswald, Jose A. Rodriguez-Rivera, James R. Neilson, Stephen D. Wilson, Elif Ertekin, Tyrel M. McQueen, and Eric S. Toberer, "New kagome prototype materials: discovery of  $\text{kv}_3\text{sb}_5$ ,  $\text{rbv}_3\text{sb}_5$ , and  $\text{csv}_3\text{sb}_5$ ," *Phys. Rev. Mater.* **3**, 094407 (2019).
- <sup>29</sup> Brenden R. Ortiz, Samuel M. L. Teicher, Yong Hu, Julia L. Zuo, Paul M. Sarte, Emily C. Schueller, A. M. Milinda Abeykoon, Matthew J. Krogstad, Stephan Rosenkranz, Raymond Osborn, Ram Seshadri, Leon Balents, Junfeng He, and Stephen D. Wil-

- son, “C<sub>5</sub>v<sub>3</sub>sb<sub>5</sub>: A  $F_2$  topological kagome metal with a superconducting ground state,” *Phys. Rev. Lett.* **125**, 247002 (2020).
- <sup>30</sup> Xiaojuan Ni, Hong Li, Feng Liu, and Jean-Luc Brédas, “Engineering of flat bands and dirac bands in two-dimensional covalent organic frameworks (cofs): relationships among molecular orbital symmetry, lattice symmetry, and electronic-structure characteristics,” *Mater. Horiz.* **9**, 88 (2022).
- <sup>31</sup> Dhaneesh Kumar, Jack Hellerstedt, Bernard Field, Benjamin Lowe, Yuefeng Yin, Nikhil V. Medhekar, and Agustin Schiffrin, “Manifestation of strongly correlated electrons in a 2d kagome metal–organic framework,” *Advanced Functional Materials* **31**, 2106474 (2021).
- <sup>32</sup> Wei Jiang, Meng Kang, Huaqing Huang, Hongxing Xu, Tony Low, and Feng Liu, “Topological band evolution between lieb and kagome lattices,” *Phys. Rev. B* **99**, 125131 (2019).
- <sup>33</sup> Jean-Philippe Lang, Haissam Hanafi, Jörg Imbrock, and Cornelia Denz, “Tilted dirac cones and asymmetric conical diffraction in photonic lieb-kagome lattices,” *Phys. Rev. A* **107**, 023509 (2023).
- <sup>34</sup> W. P. Lima, D. R. da Costa, S. H. R. Sena, and J. Milton Pereira, “Effects of uniaxial and shear strains on the electronic spectrum of lieb and kagome lattices,” *Phys. Rev. B* **108**, 125433 (2023).
- <sup>35</sup> Bin Cui, Xingwen Zheng, Jianfeng Wang, Desheng Liu, Shijie Xie, and Bing Huang, “Realization of lieb lattice in covalent-organic frameworks with tunable topology and magnetism,” *Nature Communications* **11**, 66 (2020).
- <sup>36</sup> Wei Jiang, Huaqing Huang, and Feng Liu, “A lieb-like lattice in a covalent-organic framework and its stoner ferromagnetism,” *Nature Communications* **10**, 2207 (2019).
- <sup>37</sup> Lih-King Lim, Jean-Noël Fuchs, Frédéric Piéchon, and Gilles Montambaux, “Dirac points emerging from flat bands in lieb-kagome lattices,” *Phys. Rev. B* **101**, 045131 (2020).
- <sup>38</sup> Linghao Yan, Orlando J. Silveira, Benjamin Alldritt, Ondřej Krejčí, Adam S. Foster, and Peter Liljeroth, “Synthesis and local probe gating of a monolayer metal-organic framework,” *Advanced Functional Materials* **31**, 2100519 (2021).
- <sup>39</sup> Linghao Yan, Orlando J. Silveira, Benjamin Alldritt, Shawulienu Kezilebieke, Adam S. Foster, and Peter Liljeroth, “Two-dimensional metal–organic framework on superconducting nbse<sub>2</sub>,” *ACS Nano* **15**, 17813 (2021).
- <sup>40</sup> Panagiota Perlepe, Itziar Oyarzabal, Laura Voigt, Mariusz Kubus, Daniel N. Woodruff, Sebastian E. Reyes-Lillo, Michael L. Aubrey, Philippe Négrier, Mathieu Rouzières, Fabrice Wilhelm, Andrei Rogalev, Jeffrey B. Neaton, Jeffrey R. Long, Corine Mathonière, Baptiste Vignolle, Kasper S. Pedersen, and Rodolphe Clérac, “From an antiferromagnetic insulator to a strongly correlated metal in square-lattice mcl<sub>2</sub>(pyrazine)<sub>2</sub> coordination solids,” *Nature Communications* **13**, 5766 (2022).
- <sup>41</sup> Daniel Baranowski, Marco Thaler, Dominik Brandstetter, Andreas Windischbacher, Iulia Cojocariu, Simone Mearini, Valeria Chesnyak, Luca Schio, Luca Floreano, Carolina Gutiérrez Bolaños, Peter Puschnig, Laerte L. Patera, Vitaliy Feyera, and Claus M. Schneider, “Emergence of band structure in a two-dimensional metal–organic framework upon hierarchical self-assembly,” *ACS Nano* **18**, 19618 (2024).
- <sup>42</sup> T Ohashi, S i Suga, N Kawakami, and H Tsunetsugu, “Magnetic correlations around the mott transition in the kagomé lattice hubbard model,” *Journal of Physics: Condensed Matter* **19**, 145251 (2007).
- <sup>43</sup> Ryota Higa and Kenichi Asano, “Bond formation effects on the metal-insulator transition in the half-filled kagome hubbard model,” *Phys. Rev. B* **93**, 245123 (2016).
- <sup>44</sup> Koji Kudo, Tsuneya Yoshida, and Yasuhiro Hatsugai, “Higher-order topological mott insulators,” *Phys. Rev. Lett.* **123**, 196402 (2019).
- <sup>45</sup> Takuma Ohashi, Norio Kawakami, and Hirokazu Tsunetsugu, “Mott transition in kagomé lattice hubbard model,” *Phys. Rev. Lett.* **97**, 066401 (2006).
- <sup>46</sup> N. Bulut, W. Koshibae, and S. Maekawa, “Magnetic correlations in the hubbard model on triangular and kagomé lattices,” *Phys. Rev. Lett.* **95**, 037001 (2005).
- <sup>47</sup> Josef Kaufmann, Klaus Steiner, Richard T. Scalettar, Karsten Held, and Oleg Janson, “How correlations change the magnetic structure factor of the kagome hubbard model,” *Phys. Rev. B* **104**, 165127 (2021).
- <sup>48</sup> Addressa R. Medeiros-Silva, Natanael C. Costa, and Thereza Paiva, “Thermodynamic, magnetic, and transport properties of the repulsive hubbard model on the kagome lattice,” *Phys. Rev. B* **107**, 035134 (2023).
- <sup>49</sup> G. Rohringer, H. Hafermann, A. Toschi, A. A. Katanin, A. E. Antipov, M. I. Katsnelson, A. I. Lichtenstein, A. N. Rubtsov, and K. Held, “Diagrammatic routes to nonlocal correlations beyond dynamical mean field theory,” *Rev. Mod. Phys.* **90**, 025003 (2018).
- <sup>50</sup> Josef Kaufmann, Christian Eckhardt, Matthias Pickem, Motoharu Kitatani, Anna Kauch, and Karsten Held, “Self-consistent ladder dynamical vertex approximation,” *Phys. Rev. B* **103**, 035120 (2021).
- <sup>51</sup> G. Rohringer and A. Toschi, “Impact of nonlocal correlations over different energy scales: A dynamical vertex approximation study,” *Phys. Rev. B* **94**, 125144 (2016).
- <sup>52</sup> Jonas B. Profe, Lennart Klebl, Francesco Grandi, Hendrik Hohmann, Matteo Dürrnagel, Tilman Schwemmer, Ronny Thomale, and Dante M. Kennes, “Kagome hubbard model from a functional renormalization group perspective,” *Phys. Rev. Res.* **6**, 043078 (2024).
- <sup>53</sup> Rong-Yang Sun and Zheng Zhu, “Metal-insulator transition and intermediate phases in the kagome lattice hubbard model,” *Phys. Rev. B* **104**, L121118 (2021).
- <sup>54</sup> Shashikant Singh Kunwar and Madhuparna Karmakar, “Kagome hubbard model away from the strong coupling limit: Flat band localization and non fermi liquid signatures,” (2024), [arXiv:2404.05787 \[cond-mat.str-el\]](https://arxiv.org/abs/2404.05787).
- <sup>55</sup> Shashikant Singh Kunwar and Madhuparna Karmakar, “Straintronics across lieb-kagome interconversion and variable transport scaling exponents,” *Phys. Rev. Mater.* **10**, L011002 (2026).
- <sup>56</sup> J. Hubbard, “Calculation of partition functions,” *Phys. Rev. Lett.* **3**, 77–78 (1959).
- <sup>57</sup> H. J. Schulz, “Effective action for strongly correlated fermions from functional integrals,” *Phys. Rev. Lett.* **65**, 2462–2465 (1990).
- <sup>58</sup> Simone Fratini and Sergio Ciuchi, “Displaced Drude peak and bad metal from the interaction with slow fluctuations,” *SciPost Phys.* **11**, 039 (2021).
- <sup>59</sup> Sergio Ciuchi and Simone Fratini, “Strange metal behavior from incoherent carriers scattered by local moments,” *Phys. Rev. B* **108**, 235173 (2023).
- <sup>60</sup> Chaitanya Murthy, Akshat Pandey, Ilya Esterlis, and Steven A. Kivelson, “A stability bound on the t-linear resistivity of conventional metals,” *Proceedings of the National Academy of Sciences* **120**, e2216241120 (2023).
- <sup>61</sup> N. D. Mermin and H. Wagner, “Absence of ferromagnetism or antiferromagnetism in one- or two-dimensional isotropic heisenberg models,” *Phys. Rev. Lett.* **17**, 1133–1136 (1966).
- <sup>62</sup> Tomonari Mizoguchi, Ludovic D. C. Jaubert, Roderich Moessner, and Masafumi Udagawa, “Magnetic clustering, half-moons, and shadow pinch points as signals of a proximate coulomb phase in frustrated heisenberg magnets,” *Phys. Rev. B* **98**, 144446 (2019).

- (2018).
- 63 M. E. Zhitomirsky, “Octupolar ordering of classical kagome antiferromagnets in two and three dimensions,” *Phys. Rev. B* **78**, 094423 (2008).
  - 64 Han Yan, Rico Pohle, and Nic Shannon, “Half moons are pinch points with dispersion,” *Phys. Rev. B* **98**, 140402 (2018).
  - 65 Dominik Kiese, Francesco Ferrari, Nikita Astrakhantsev, Nils Niggemann, Pratyay Ghosh, Tobias Müller, Ronny Thomale, Titus Neupert, Johannes Reuther, Michel J. P. Gingras, Simon Trebst, and Yasir Iqbal, “Pinch-points to half-moons and up in the stars: The kagome skymap,” *Phys. Rev. Res.* **5**, L012025 (2023).
  - 66 Steven T. Bramwell and Michel J. P. Gingras, “Spin ice state in frustrated magnetic pyrochlore materials,” *Science* **294**, 1495 (2001).
  - 67 T. Fennell, P. P. Deen, A. R. Wildes, K. Schmalzl, D. Prabhakaran, A. T. Boothroyd, R. J. Aldus, D. F. McMorrow, and S. T. Bramwell, “Magnetic coulomb phase in the spin ice  $\text{Ho}_2\text{Ti}_2\text{O}_7$ ,” *Science* **326**, 415 (2009).
  - 68 S. Gao, K. Guratinder, U. Stuhr, J. S. White, M. Mansson, B. Roessli, T. Fennell, V. Tsurkan, A. Loidl, M. Ciomaga Hatnean, G. Balakrishnan, S. Raymond, L. Chapon, V. O. Garlea, A. T. Savici, A. Cervellino, A. Bombardi, D. Chernyshov, Ch. Rüegg, J. T. Haraldsen, and O. Zaharko, “Manifolds of magnetic ordered states and excitations in the almost heisenberg pyrochlore antiferromagnet  $\text{MgCr}_2\text{O}_4$ ,” *Phys. Rev. B* **97**, 134430 (2018).
  - 69 Elliott H. Lieb, “Two theorems on the hubbard model,” *Phys. Rev. Lett.* **62**, 1201–1204 (1989).
  - 70 Linda Ye, Shiang Fang, Mingu Kang, Josef Kaufmann, Yonghun Lee, Caolan John, Paul M. Neves, S. Y. Frank Zhao, Jonathan Denlinger, Chris Jozwiak, Aaron Bostwick, Eli Rotenberg, Efthimios Kaxiras, David C. Bell, Oleg Janson, Riccardo Comin, and Joseph G. Checkelsky, “Hopping frustration-induced flat band and strange metallicity in a kagome metal,” *Nature Physics* **20**, 610 (2024).
  - 71 Lei Chen, Fang Xie, Shouvik Sur, Haoyu Hu, Silke Paschen, Jennifer Cano, and Qimiao Si, “Emergent flat band and topological kondo semimetal driven by orbital-selective correlations,” *Nature Communications* **15**, 5242 (2024).
  - 72 Andrej Pustogow, Yohei Saito, Anja Löhle, Miriam Sanz Alonso, Atsushi Kawamoto, Vladimir Dobrosavljević, Martin Dressel, and Simone Fratini, “Rise and fall of landau’s quasiparticles while approaching the mott transition,” *Nature Communications* **12**, 1571 (2021).
  - 73 Riku Yamamoto, Tetsuya Furukawa, Kazuya Miyagawa, Takahiko Sasaki, Kazushi Kanoda, and Tetsuaki Itou, “Electronic griffiths phase in disordered mott-transition systems,” *Phys. Rev. Lett.* **124**, 046404 (2020).
  - 74 Elias Lahoud, O. Nganba Meetei, K. B. Chaska, A. Kanigel, and Nandini Trivedi, “Emergence of a novel pseudogap metallic state in a disordered 2d mott insulator,” *Phys. Rev. Lett.* **112**, 206402 (2014).
  - 75 Tingxin Li, Shengwei Jiang, Lizhong Li, Yang Zhang, Kaifei Kang, Jiacheng Zhu, Kenji Watanabe, Takashi Taniguchi, Debanjan Chowdhury, Liang Fu, Jie Shan, and Kin Fai Mak, “Continuous mott transition in semiconductor moirésuperlattices,” *Nature* **597**, 350 (2021).
  - 76 Augusto Ghiotto, En-Min Shih, Giancarlo S. S. G. Pereira, Daniel A. Rhodes, Bumho Kim, Jiawei Zang, Andrew J. Millis, Kenji Watanabe, Takashi Taniguchi, James C. Hone, Lei Wang, Cory R. Dean, and Abhay N. Pasupathy, “Quantum criticality in twisted transition metal dichalcogenides,” *Nature* **597**, 345 (2021).
  - 77 E. Uykur, B. R. Ortiz, O. Iakutkina, M. Wenzel, S. D. Wilson, M. Dressel, and A. A. Tsirlin, “Low-energy optical properties of the nonmagnetic kagome metal  $\text{CsV}_3\text{Sb}_5$ ,” *Phys. Rev. B* **104**, 045130 (2021).
  - 78 Luca V. Delacrétaz, Blaise Goutéraux, Sean A. Hartnoll, and Anna Karlsson, *SciPost Phys.* **3**, 025 (2017).
  - 79 S. Caprara, C. Di Castro, S. Fratini, and M. Grilli, “Anomalous optical absorption in the normal state of overdoped cuprates near the charge-ordering instability,” *Phys. Rev. Lett.* **88**, 147001 (2002).
  - 80 O. Gunnarsson, M. Calandra, and J. E. Han, “Colloquium: Saturation of electrical resistivity,” *Rev. Mod. Phys.* **75**, 1085–1099 (2003).
  - 81 K. Takenaka N. E. Hussey || and H. Takagi, “Universality of the mott–ioffe–regel limit in metals,” *Philosophical Magazine* **84**, 2847 (2004).
  - 82 Xiaoyu Deng, Jernej Mravlje, Rok Žitko, Michel Ferrero, Gabriel Kotliar, and Antoine Georges, “How bad metals turn good: Spectroscopic signatures of resilient quasiparticles,” *Phys. Rev. Lett.* **110**, 086401 (2013).
  - 83 Christophe Berthod, Jernej Mravlje, Xiaoyu Deng, Rok Žitko, Dirk van der Marel, and Antoine Georges, “Non-drude universal scaling laws for the optical response of local fermi liquids,” *Phys. Rev. B* **87**, 115109 (2013).
  - 84 Edwin W. Huang, Ryan Sheppard, Brian Moritz, and Thomas P. Devereaux, “Strange metallicity in the doped hubbard model,” *Science* **366**, 987 (2019).
  - 85 J. Vučićević, D. Tanasković, M. J. Rozenberg, and V. Dobrosavljević, “Bad-metal behavior reveals mott quantum criticality in doped hubbard models,” *Phys. Rev. Lett.* **114**, 246402 (2015).
  - 86 Simone Fratini, Arnaud Ralko, and Sergio Ciuchi, “Strange metal transport from coupling to fluctuating spins,” (2024), [arXiv:2412.04322 \[cond-mat.str-el\]](https://arxiv.org/abs/2412.04322).
  - 87 R. Rösslhuber, R. Hübner, M. Dressel, and A. Pustogow, “Pressure-dependent dielectric response of the frustrated mott insulator  $\kappa$ -(BEDT-TTF) $_2\text{Ag}_2(\text{CN})_3$ ,” *Phys. Rev. B* **107**, 075113 (2023).
  - 88 P. Gegenwart, C. Langhammer, C. Geibel, R. Helfrich, M. Lang, G. Sparn, F. Steglich, R. Horn, L. Donnevert, A. Link, and W. Assmus, “Breakup of heavy fermions on the brink of “phase A” in  $\text{CeCu}_2\text{Si}_2$ ,” *Phys. Rev. Lett.* **81**, 1501–1504 (1998).
  - 89 O. Trovarelli, C. Geibel, S. Mederle, C. Langhammer, F. M. Grosche, P. Gegenwart, M. Lang, G. Sparn, and F. Steglich, “ $\text{YbRh}_2\text{Si}_2$ : Pronounced non-fermi-liquid effects above a low-lying magnetic phase transition,” (2000).
  - 90 S R Julian, C Pfeleiderer, F M Grosche, N D Mathur, G J McMullan, A J Diver, I R Walker, and G G Lonzarich, “The normal states of magnetic d and f transition metals,” *Journal of Physics: Condensed Matter* **8**, 9675 (1996).
  - 91 P Coleman, C Pépin, Qimiao Si, and R Ramazashvili, “How do fermi liquids get heavy and die?” *Journal of Physics: Condensed Matter* **13**, R723 (2001).
  - 92 Niravkumar D. Patel, Anamitra Mukherjee, Nitin Kaushal, Adriana Moreo, and Elbio Dagotto, “Non-fermi liquid behavior and continuously tunable resistivity exponents in the anderson-hubbard model at finite temperature,” *Phys. Rev. Lett.* **119**, 086601 (2017).
  - 93 Y. Imry, *Introduction to Mesoscopic Physics* (Oxford University Press).
  - 94 Shin-ichi Kimura, Muhammad Frassetia Lubis, Hiroshi Watanabe, Yasuyuki Shimura, and Toshiro Takabatake, “Anisotropic non-fermi liquid and dynamical planckian scaling of a quasi-kagome kondo lattice system,” *npj Quantum Materials* **10**, 85 (2025).

- <sup>95</sup> Evgeny Mikheev, Adam J. Hauser, Burak Himmetoglu, Nelson E. Moreno, Anderson Janotti, Chris G. Van de Walle, and Susanne Stemmer, “Tuning bad metal and non-fermi liquid behavior in a mott material: Rare-earth nickelate thin films,” *Science Advances* **1**, e1500797 (2015).
- <sup>96</sup> E. Abrahams, P. W. Anderson, D. C. Licciardello, and T. V. Ramakrishnan, “Scaling theory of localization: Absence of quantum diffusion in two dimensions,” *Phys. Rev. Lett.* **42**, 673–676 (1979).
- <sup>97</sup> Benjamin Lowe, Bernard Field, Jack Hellerstedt, Julian Ceddia, Henry L. Nourse, Ben J. Powell, Nikhil V. Medhekar, and Agustin Schiffrin, “Local gate control of mott metal-insulator transition in a 2d metal-organic framework,” *Nature Communications* **15**, 3559 (2024).
- <sup>98</sup> Bernard Field, Agustin Schiffrin, and Nikhil V. Medhekar, “Correlation-induced magnetism in substrate-supported 2d metal-organic frameworks,” *npj Computational Materials* **8**, 227 (2022).
- <sup>99</sup> T. Takenaka, K. Ishihara, M. Roppongi, Y. Miao, Y. Mizukami, T. Makita, J. Tsurumi, S. Watanabe, J. Takeya, M. Yamashita, K. Torizuka, Y. Uwatoko, T. Sasaki, X. Huang, W. Xu, D. Zhu, N. Su, J.-G. Cheng, T. Shibauchi, and K. Hashimoto, “Strongly correlated superconductivity in a copper-based metal-organic framework with a perfect kagome lattice,” *Science Advances* **7**, eabf3996 (2021).
- <sup>100</sup> Maximilian A. Springer, Tsai-Jung Liu, Agnieszka Kuc, and Thomas Heine, “Topological two-dimensional polymers,” *Chem. Soc. Rev.* **49**, 2007 (2020).
- <sup>101</sup> Mingchao Wang, Renhao Dong, and Xinliang Feng, “Two-dimensional conjugated metal–organic frameworks (2d c-mofs): chemistry and function for moftronics,” *Chem. Soc. Rev.* **50**, 2764 (2021).